

# Cornichon2 Dictates the Time Course of Excitatory Transmission at Individual Hippocampal Synapses

Sami Boudkkazi,<sup>1</sup> Aline Brechet,<sup>1</sup> Jochen Schwenk,<sup>1,2</sup> and Bernd Fakler<sup>1,2,\*</sup>

<sup>1</sup>Institute of Physiology, University of Freiburg, Hermann-Herder-Str. 7, 79104 Freiburg, Germany

<sup>2</sup>Center for Biological Signalling Studies (BIOS), Albertstr. 10, 79104 Freiburg, Germany

\*Correspondence: [bernd.fakler@physiologie.uni-freiburg.de](mailto:bernd.fakler@physiologie.uni-freiburg.de)

<http://dx.doi.org/10.1016/j.neuron.2014.03.031>

## SUMMARY

*Cornichon2* (CNIH2), an integral component of AMPA receptor (AMPA) complexes in the mammalian brain, slows deactivation and desensitization of heterologously reconstituted receptor channels. Its significance in neuronal signal transduction, however, has remained elusive. Here we show by paired recordings that CNIH2-containing AMPARs dictate the slow decay of excitatory postsynaptic currents (EPSCs) elicited in hilar mossy cells of the hippocampus by single action potentials in mossy fiber boutons (MFB). Selective knockdown of CNIH2 markedly accelerated EPSCs in individual MFB-mossy cell synapses without altering the EPSC amplitude. In contrast, the rapidly decaying EPSCs in synapses between MFBs and aspiny interneurons that lack expression of CNIH2 were unaffected by the protein knockdown but were slowed by virus-directed expression of CNIH2. These results identify CNIH2 as the molecular distinction between slow and fast EPSC phenotypes and show that CNIH2 influences the time course and, hence, the efficacy of excitatory synaptic transmission.

## INTRODUCTION

Fast excitatory neurotransmission in the brain is primarily driven by postsynaptic AMPA-type glutamate receptors (AMPA). Activated upon glutamate release from presynaptic boutons, AMPARs provide the transient excitatory postsynaptic currents (EPSCs) required for propagation of the electrical signal (Raman and Trussell, 1992; Sah et al., 1990; Silver et al., 1992). Efficacy and reliability of the signal propagation are variable among CNS neurons and are directly related to the time course and amplitude of the EPSCs (Conti and Weinberg, 1999; Geiger et al., 1995; Isaac et al., 2007; Trussell, 1999). Both of these properties are shaped by the gating kinetics of the AMPARs and thus depend on the molecular composition of the receptor channels (Farrant and Cull-Candy, 2010; Jonas, 2000; Milstein et al., 2007; Mosbacher et al., 1994).

Native AMPARs in the mammalian brain are macromolecular complexes of considerable diversity assembled from a pool of more than 30 different protein constituents (Schwenk et al.,

2012). Gating and pore properties of all AMPARs are determined by the receptor-core that is built from tetramers of the pore-forming GluA1-4 proteins (Hollmann and Heinemann, 1994; Seeburg, 1993; Sobolevsky et al., 2009), the transmembrane AMPAR regulatory proteins (TARPs,  $\gamma$ -2,  $\gamma$ -3,  $\gamma$ -4,  $\gamma$ -5,  $\gamma$ -7, and  $\gamma$ -8; Milstein et al., 2007; Tomita et al., 2003), and the *cornichon* homologs 2 (CNIH2) and 3 (CNIH3) (Schwenk et al., 2009). In heterologous expression experiments, both TARPs and CNIHs impact the gating of the AMPARs, either alone or in combination, by distinctly slowing deactivation and desensitization of various GluA homo- or hetero-tetramers (Schwenk et al., 2009; Shi et al., 2010). Among the auxiliary core subunits, the two CNIH proteins exert the strongest influence, slowing the time constants of either channel closing process by up to more than 5-fold, independent of the GluA composition of the pore (Coombs et al., 2012; Schwenk et al., 2009; Shi et al., 2010).

Notwithstanding the profound effects on AMPAR gating in heterologous systems, the significance of the CNIH proteins for EPSCs and synaptic transmission has remained unclear. Recent work using genetic deletion of the CNIHs reported accelerated miniature EPSCs in hippocampal CA1 pyramidal cells as a result of an altered GluA subunit composition of synaptic AMPARs promoted by exclusive interaction of CNIHs with GluA1 (Herring et al., 2013). Such selectivity in CNIH-GluA association, however, is in strict contrast to proteomic and biochemical analyses demonstrating equally robust assembly of the CNIH proteins into AMPARs in the absence of GluA1 or GluA2 proteins (Schwenk et al., 2012) (Figure S1 available online). For investigating the relevance of CNIHs in excitatory synaptic transmission, we, therefore, turned to two types of neurons for which spontaneous EPSCs with markedly different time courses have been reported: mossy cells and aspiny interneurons in the hilar region of the rat hippocampus (Livsey and Vicini, 1992).

Here we investigated the role of CNIHs in synaptic transmission using paired recordings between presynaptic terminals and postsynaptic target cells together with knockdown of protein expression by virally delivered shRNA. We show that CNIH2 profoundly impacts the timing of synaptic transmission in hippocampal hilar mossy cells and identify CNIH2 as the molecular distinction between slow and fast EPSC phenotypes.

## RESULTS

### Recording of EPSCs in Individual Synapses

To measure the time course of synaptic transmission, we used paired recordings between presynaptic mossy fiber boutons

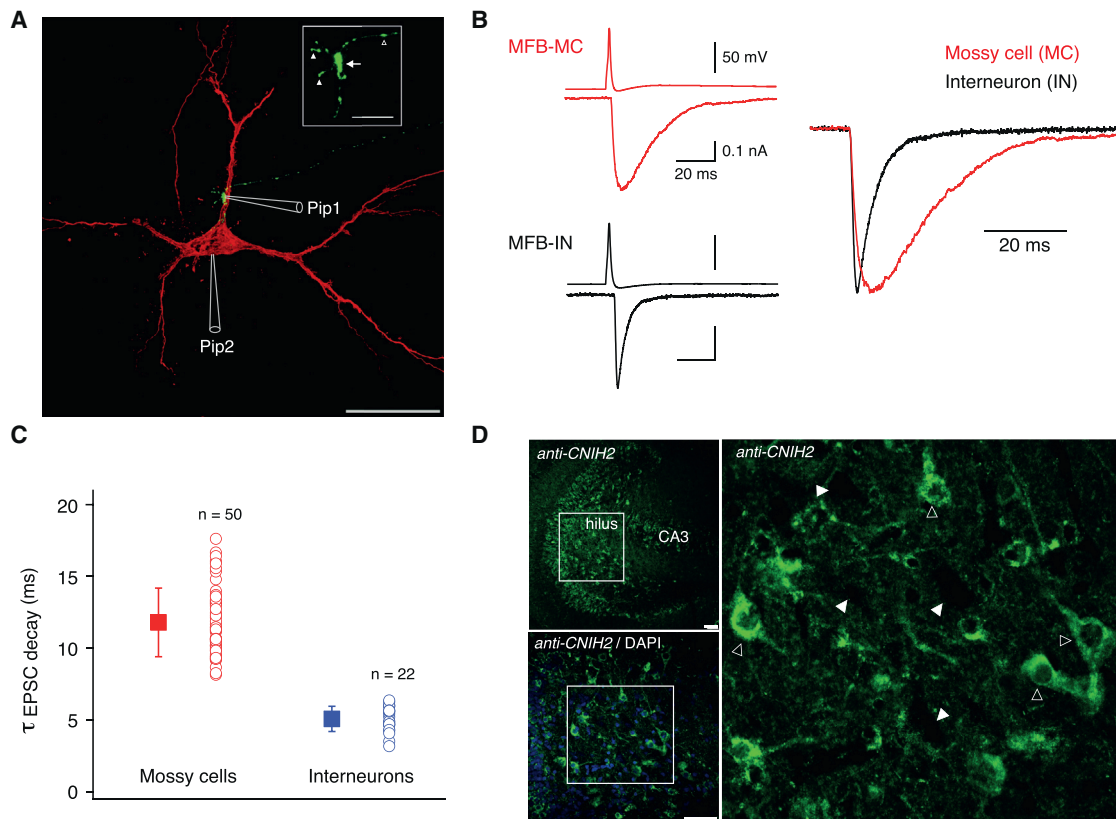


**Figure 1. Hilar Mossy Cells and Aspiny Interneurons Differ in EPSC Time Course and Expression of CNIH2**

(A) Confocal fluorescence image illustrating the paired recording configuration at a MFB-mossy cell synapse. Both MFB and mossy cell were filled with dyes (biocytin [mossy cell, red]; alexa 488 [MFB, green]) via the patch pipettes (Pip1 and Pip2). Inset: MFB at enlarged scale illustrating axon (open arrowhead), main body (arrow), and filopodia (filled arrowhead; Acsády et al., 1998); scale bar is 10  $\mu$ m.

(B) Left panel: representative AP and EPSC traces determined by paired recordings at a MFB-mossy cell (upper) or MFB-interneuron synapse (lower). Right panel: overlay of the normalized EPSCs shown on the left. Scaling for time, current, and voltage, as indicated.

(C) Summary plots of the mean ( $\pm$ SD)  $\tau_{EPSC\ decay}$  values determined by mono-exponential fits to evoked EPSCs recorded in 50 mossy cells and 22 interneurons. Squares represent mean  $\pm$ SD of the individual  $\tau_{EPSC\ decay}$  values.

(D) Confocal fluorescence images of a slice section covering the hilar region of the hippocampus stained with DAPI (blue) and an anti-CNIH2 antibody (green). Framed parts of the images are shown at enlarged scale on the lower left (frame from the upper left image) and on the right (frame from the lower left). Open arrowheads denote large CNIH2-expressing neurons, filled arrowheads denote neurons devoid of CNIH2 protein. Scale bars are 50  $\mu$ m.

(MFBs) and postsynaptic mossy cells or aspiny interneurons (Experimental Procedures). The MFBs, large presynaptic terminals of the dentate gyrus granule cells, are amenable to patch-clamp recordings (Bischofberger et al., 2006; Geiger and Jonas, 2000; Szabadics and Soltesz, 2009) and were, by functional (see below) and morphological approaches, found to contact both mossy cells and aspiny interneurons (Acsády et al., 1998) (Figure 1A). In slice experiments, the latter were identified by their action potential phenotype (Livsey and Vicini, 1992) and their structural characteristics (Acsády et al., 1998; Amaral, 1978; Frotscher et al., 1991) together with retrograde dye-filling and postrecording confocal microscopy (Figures 1A, 2A, and 4A).

Figure 1 illustrates paired recordings in MFB-mossy cell and MFB-interneuron synapses. Single presynaptic APs elicited by brief current pulses evoked robust EPSCs in either type of postsynaptic neuron demonstrating functional connectivity in both synapses (Figure 1A). The EPSCs, recorded at a holding potential of  $-70$  mV, exhibited comparable amplitudes in both synap-

ses (mean values of  $\sim 300$  pA and  $\sim 200$  pA obtained in 50 mossy cells and 22 interneurons, respectively) and were entirely mediated by AMPARs as revealed by their complete block by 10  $\mu$ M CNQX (data not shown). The time courses of the EPSCs obtained from MFB-mossy cell and MFB-interneuron synapses, however, were quite distinct, displaying obvious differences in onset and decay kinetics (Figure 1B). Most prominently, the decay phase of the mossy cell EPSCs was prolonged over that in interneurons. Mono-exponential fits to the current decay recorded in 50 MFB-mossy cell and 22 MFB-interneuron synapses yielded mean values ( $\pm$ SD) for the decay time constant ( $\tau_{EPSC\ decay}$ ) of  $11.8 \pm 2.4$  ms and  $5.1 \pm 0.9$  ms, respectively (Figure 1C). Noteworthy, the values determined for  $\tau_{EPSC\ decay}$  in either type of postsynaptic neuron revealed considerable variation among cells and/or synapses (values of 8.1 to 17.7 ms and of 3.1 to 6.3 ms in mossy cells and interneurons, respectively), while the EPSCs recorded in any individual synapse were rather invariable (SD values  $< 1$  ms; Figure 1C).

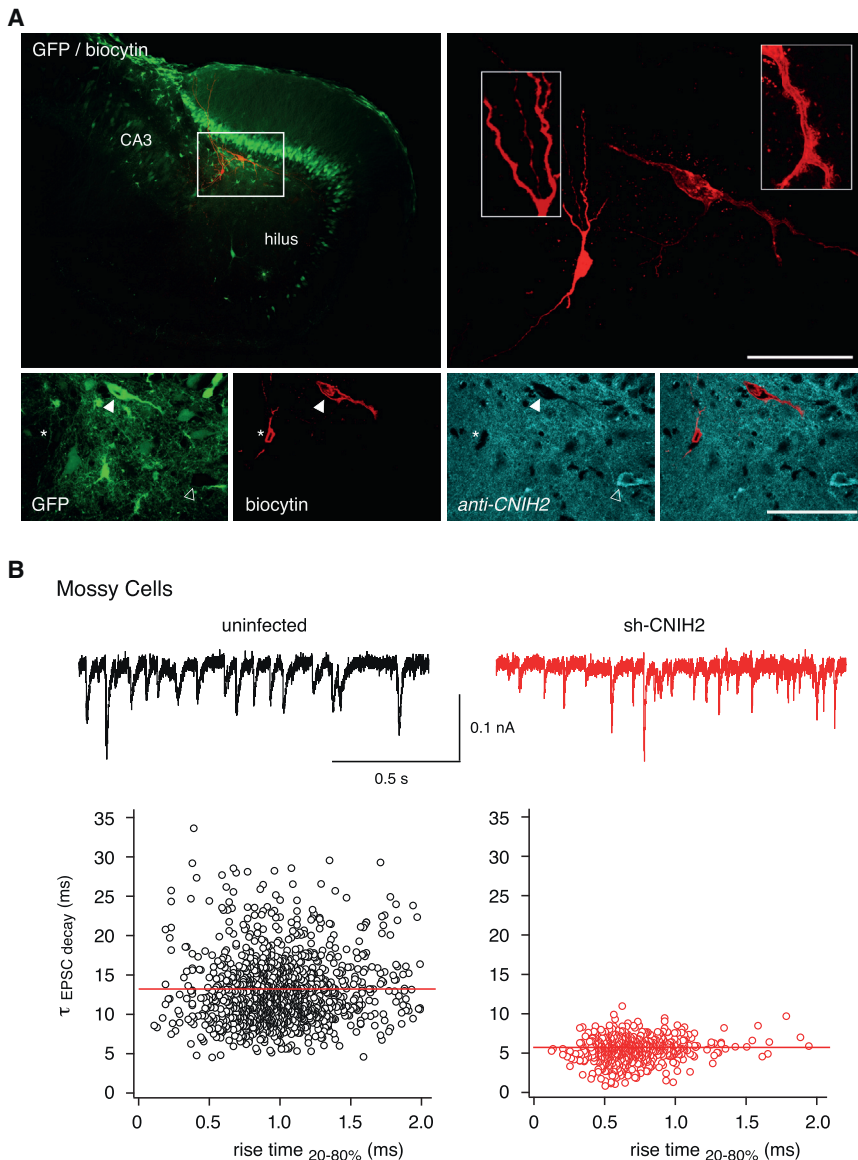


**Figure 2. Knockdown of CNIH2 Accelerates the Decay of Spontaneous EPSCs in a Mossy Cell**

(A) Upper-left panel: confocal fluorescence image of a hippocampal slice section obtained from an animal injected with the sh-CNIH2 lentivirus. GFP fluorescence indicates transduced cells; red fluorescence originates from a mossy cell and an interneuron used for patch-clamp recordings and filled with biocytin. Upper right panel: mossy cell (horizontal) and aspiny interneuron (boxed frame on the left) at enlarged scale. Insets illustrate proximal dendrites with characteristic features of either cell type (thorny excrescences [mossy cell] and aspiny dendrites [interneuron]). Lower panels: framed box from the upper left displayed at enlarged scale and viewed through different filters to reveal the distinct fluorescence sources given at the bottom; image on the right is a merge of the two images in the middle. Staining by *anti-CNIH2* is shown in cyan and originates from the Alexa633-conjugated secondary antibody whose fluorescence is acquired on the red channel. Scale bars are 50  $\mu\text{m}$ . Note the lack of CNIH2 staining in both the transduced mossy cell (filled triangle, GFP positive) and the interneuron (asterisk), while a nontransduced (GFP negative) mossy cell (open triangle) displays robust CNIH2 expression. (B) Upper panel: spontaneous EPSCs recorded from an uninfected (left panel) and a sh-CNIH2-transduced mossy cell (right panel). Time and current scaling as indicated. Lower panel: plot of  $\tau$  EPSC decay versus rise time  $_{20\%-80\%}$  determined in 1,319 (open dots, left) and 785 single EPSCs (right) from the cells above. Red lines are linear fits to the data points with y values of 13.2 ms (left) and 5.8 ms (right).

These recordings were complemented by immunocytochemistry on hippocampal slices stained with DAPI and a CNIH2-specific antibody (*anti-CNIH2*, [Experimental Procedures](#)). As shown in [Figure 1D](#), CNIH2 immunoreactivity was detected in soma and dendrites of a subset of large hilar neurons (open arrowheads), presumably mossy cells, while neighboring neurons were not stained (filled arrowheads).

Together, these results prompted the hypothesis that the slow EPSC decay in mossy cells results from slow deactivation/desensitization processes exerted by assembly of CNIH2 into the core of synaptic AMPARs.

#### CNIH2 Knockdown Speeds Mossy Cell EPSC Kinetics

To test this hypothesis, we examined the significance of CNIH2 for the gating of synaptic AMPARs and the EPSC time course by means of knocking down its expression through lentivirus-

mediated short hairpin RNA (sh-CNIH2). CNIH2 was targeted because, in the hippocampus, the amount of CNIH2 protein exceeds that of CNIH3 by at least an order of magnitude (data not shown). When tested on hippocampal cultures, quantification of protein amounts by western blotting and high-resolution mass spectrometry (MS) ([Bildl et al., 2012](#); [Schwenk et al., 2012](#)) showed that sh-CNIH2 mediated a close to complete knockdown of its target ([Figure S2](#)). Moreover, protein knockdown was highly specific, as neither unrelated proteins nor the protein amounts of other AMPAR core constituents, most notably the GluA1-4 proteins, TARP  $\gamma$ -8, or CNIH3, were affected by sh-CNIH2 ([Figure S2](#)). The sh-CNIH2 lentivirus, which also expresses GFP, was stereotactically delivered by transcranial injection into the dentate gyrus of rat hippocampi (at P6/P7) that were used for subsequent slice experiments 10 to 18 days later. As visualized by the GFP marker, the virus transduced both mossy cells and interneurons in the hilus ([Figure 2A](#), lower panel), and the GFP expression was used to guide slice recordings.

In a first set of experiments, we used the whole-cell configuration on hilar mossy cells to record single EPSCs ([Figure 2B](#),

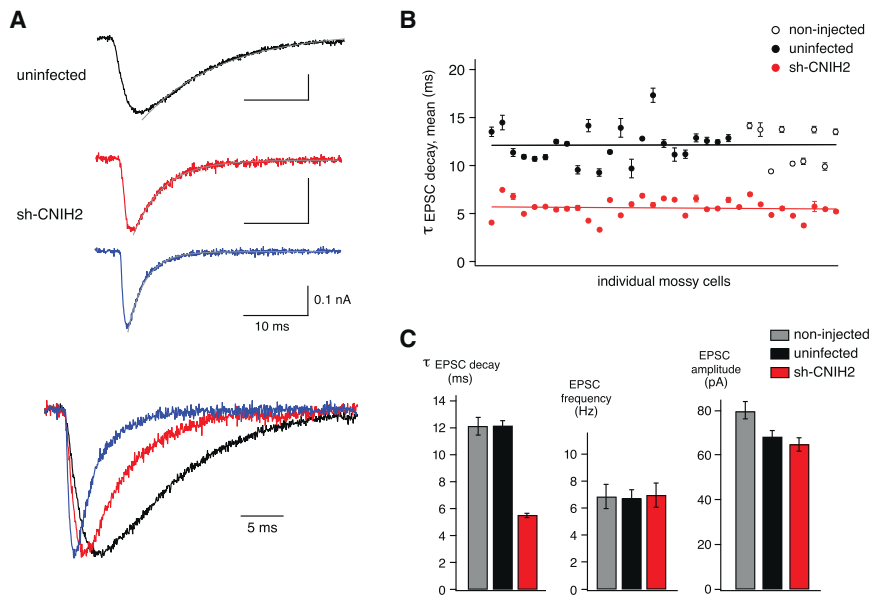


**Figure 3. CNIH2 Knockdown Decreases the Decay Time Constant without Affecting Amplitude and Frequency of EPSCs**

(A) Single EPSCs recorded from the two cells in Figure 2. Lines represent results of mono-exponential fits to the current decay with values for  $\tau_{\text{EPSC decay}}$  of 12.3 ms (uninfected), 4.7 ms (sh-CNIH2 transduced, red), and 2.7 ms (sh-CNIH2 transduced, blue). Time and current scaling as indicated.

(B) Plot of the mean values ( $\pm$ SEM) of  $\tau_{\text{EPSC decay}}$  obtained from individual mossy cells that were either transduced with sh-CNIH2 (red) or were uninfected controls. Lines are results of a linear fit to the data with y values of 12.1 ms (controls) and 5.6 ms (sh-CNIH2 transduced). All mean values were derived from 157 to 1,319 single EPSCs.

(C) Bar graph summarizing the analyses of the indicated EPSC parameters. Bars represent mean  $\pm$ SEM of 44 (uninfected), 14 (noninjected), and 50 (sh-CNIH2-transduced) mossy cells. Note the selective effect of sh-CNIH2 on the  $\tau_{\text{EPSC decay}}$ .

upper panel; Figure 3A) evoked by the frequent spontaneous APs occurring in the numerous synapses contacting these cells (Buckmaster et al., 1996). Figure 2B (lower panel) illustrates results from two representative mossy cells that reflect the clear differences between neurons transduced with sh-CNIH2 and the control. First, the values for  $\tau_{\text{EPSC decay}}$  obtained in the uninfected mossy cell extended over a broad range, between 5 ms and 30 ms with a mean value ( $\pm$ SD) of  $12.8 \pm 4.1$  ms ( $n = 1,319$  EPSCs; Figure 2B, left panel). In contrast, in the transduced neuron where knockdown of the CNIH2 protein was virtually complete as verified by postrecording confocal microscopy using GFP fluorescence, biocytin-labeling, and anti-CNIH2 staining (Figure 2A, lower panel; Figure S3), both the range and the absolute values of  $\tau_{\text{EPSC decay}}$  were markedly altered. The mean  $\tau_{\text{EPSC decay}}$  decreased to  $5.5$  ms ( $\pm 1.4$  ms,  $n = 785$  EPSCs), and the distribution was largely narrowed with individual values of  $\tau_{\text{EPSC decay}}$  ranging from about 1.5 ms to 9 ms (Figure 2B, right panel). Second, concomitant with the speeded decay kinetics, the rise-time of the EPSCs (rise time<sub>20%–80%</sub>) also appeared faster in the CNIH2 knockdown neuron (mean values of  $0.99 \pm 0.32$  ms and  $0.69 \pm 0.23$  ms), most likely as a result of the accelerated EPSC decay as observed above for the EPSCs of mossy cells versus aspiny interneurons and for GluA tetramers with and without coassembled CNIH2 (Figures 2B and 3A) (Schwenk et al., 2009).

Recordings from an additional 32 mossy cells under control conditions, either uninfected (23 cells) or from noninjected brains (9 cells), and 32 sh-CNIH2 transduced mossy cells corroborated the marked effect of the CNIH2 knockdown on the timing of the EPSCs. Thus, the mean values obtained for  $\tau_{\text{EPSC decay}}$  in control mossy cells ranged from 9.3 ms to 17.3 ms and yielded an overall mean ( $\pm$ SEM) of  $12.1 \pm 0.6$  ms (uninfected or noninjected), numbers closely matching the values obtained from the evoked EPSCs in paired recordings (Figure 1C). The knockdown of CNIH2 verified by post hoc analyses (Figure S3) led to a decreased mean  $\tau_{\text{EPSC decay}}$  of  $5.6 \pm 0.2$  ms with a markedly

smaller range for the mean values of individual cells (3.3 ms to 7.3 ms; Figure 3B). Strikingly, both the range and the mean value of  $\tau_{\text{EPSC decay}}$  were similar to the values obtained from interneurons that lack expression of CNIH2 (Figures 1 and 2A).

While CNIH2 clearly affected EPSC kinetics, neither the amplitude nor the frequency of single EPSCs was altered (Figure 3C), in line with the result that CNIH2 knockdown did not change the expression of GluA proteins or other AMPAR core constituents (Figure S2).

As an additional control, we repeated the experiments with lentiviruses where sh-CNIH2 was either not present (GFP-virus, 17 cells) or replaced by a scrambled shRNA designed to not target any gene transcript (sh-control, Alberich-Jordà et al., 2012; 6 cells). In both cases, the results were very similar and did not display any difference to uninfected mossy cells in all parameters evaluated including mean and distribution of  $\tau_{\text{EPSC decay}}$ , rise-time or amplitude of the EPSCs (Figure 4).

Together, these results indicated that when CNIH2 is a component of synaptic AMPARs, it dictates the slow decay of EPSCs in hilar mossy cells.

#### Lack of Effect of CNIH2 shRNA on Interneuron EPSCs

If CNIH2-containing AMPARs determine the slow kinetics of hilar mossy cell EPSCs, and the fast EPSCs in aspiny interneurons reflect a lack of CNIH2, then EPSC kinetics in aspiny interneurons should not be affected by the sh-CNIH2. This was probed in transduced and uninfected interneurons by recording spontaneous EPSCs that, also in this type of hilar neuron, occurred at high frequencies (Livsey and Vicini, 1992) (Figure 5A).

Analyses of the kinetic properties of large numbers of single EPSCs (Figure 5B) in a total of 28 interneurons showed virtually identical results for transduced cells and uninfected controls (Figures 5A–5D). This is demonstrated by  $\tau_{\text{EPSC decay}}$  versus rise time<sub>20%–80%</sub> plots that displayed very similar scattering ranges (Figure 5A), as well as by the mean values of the  $\tau_{\text{EPSC decay}}$  obtained in 12 transduced and 16 uninfected

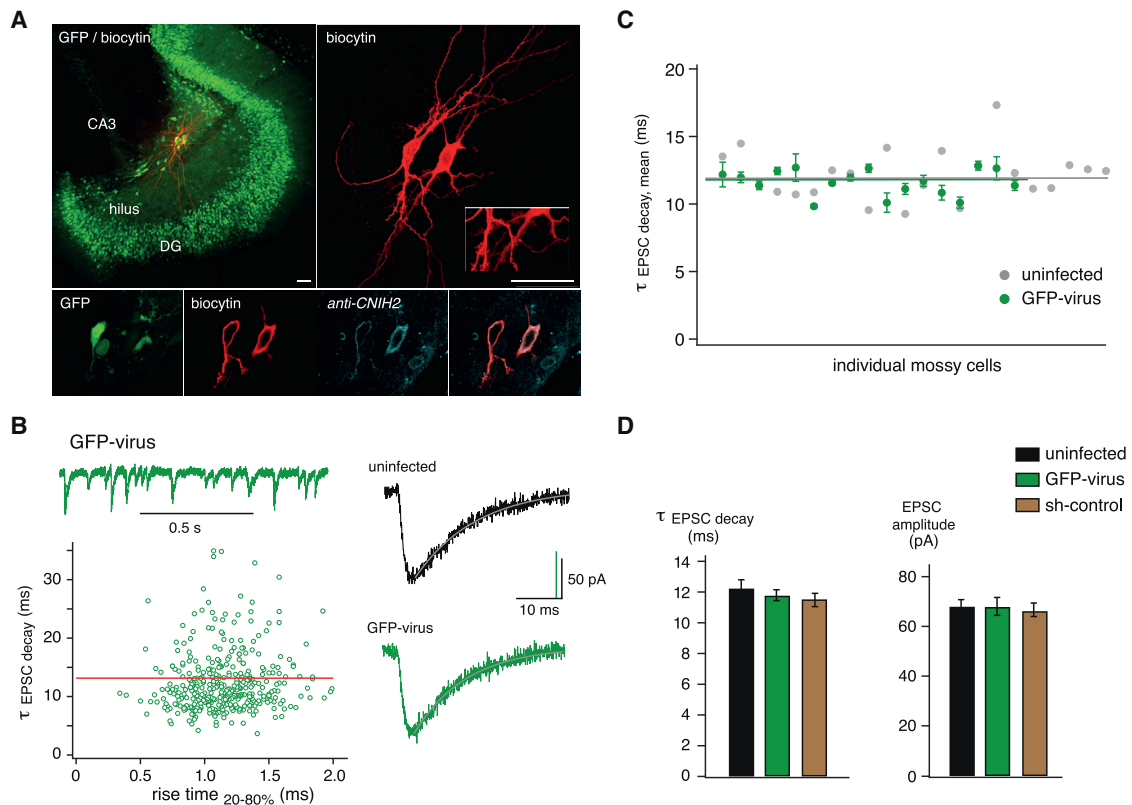


**Figure 4. Control Viruses Do Not Affect Mossy Cell EPSCs**

(A) Confocal fluorescence images of a hippocampal slice section as in Figure 2 obtained from an animal that was injected with a GFP-expressing control virus. Upper panel: red fluorescence originates from two mossy cells, either transduced (left cell) or uninfected (right cell), used for patch-clamp recordings and filled with biocyten. Inset: proximal dendrites of both cells at enlarged scale. Note the intact thorny excrescences on both cells. Lower panel: the two cells imaged with the indicated fluorescence source. Scale bars are 50  $\mu$ m. Note expression of CNIH2 (cyan) in both neurons.

(B) Spontaneous EPSC recording, representative single EPSCs, and a  $\tau$  EPSC decay versus rise time  $_{20\%-80\%}$  plot as in Figures 2 and 3.

(C) Plot of the mean values ( $\pm$ SEM) of  $\tau$  EPSC decay obtained from individual mossy cells transduced with the GFP-virus and from uninfected mossy cells. Line is a linear fit with a y value of 12.1 ms. Mean values were derived from 62 to 2,027 single EPSCs.

(D) Bar graph as in Figure 3C for the indicated mossy cells. Bars represent mean  $\pm$ SEM of 44 (uninfected), 17 (GFP-virus), and 10 (sh-control) mossy cells. Note the lack of effect of both controls.

interneurons (Figure 5C). The latter yielded identical overall mean values of  $4.7 \pm 1.2$  ms (sh-CNIH2) and  $4.6 \pm 1.2$  ms (uninfected/non-injected) and thus closely resembled the results from sh-CNIH2-transduced mossy cells (Figure 3). Similarly, the rise time (values of  $0.61 \pm 0.19$  ms and  $0.62 \pm 0.12$  ms) and the EPSC frequency did not display significant differences (Figure 5D). Merely, the EPSC amplitudes appeared slightly smaller in all transduced interneurons (including those transduced with control viruses) compared to uninfected controls (Figure 5D).

Taken together, these results indicated that CNIH2 endows characteristic EPSC timing in a cell-type-specific manner and identify a molecular mechanism to distinctly shape synaptic transmission in mossy cells and aspiny interneurons in the hilar region of the hippocampus.

### Expression of CNIH2 Converts EPSC Phenotype in Interneurons

Next, we investigated whether CNIH2 may endow neurons with the slow EPSC phenotype observed in mossy cells. For this

purpose, the CNIH2 protein was expressed in interneurons by delivery of a lentivirus (Experimental Procedures) (Gascón et al., 2008).

The spontaneous EPSCs recorded from two representative hilar interneurons (Figure 6A, upper panel), one transduced with the virus driving CNIH2 expression (+CNIH2) and the other a noninfected control cell, together with the respective scatter-plots of  $\tau$  EPSC decay versus rise time  $_{20\%-80\%}$  illustrate the profound effect of the exogenous CNIH2 expression (Figure 6A, lower panel). Both the mean and the scattering range of the  $\tau$  EPSC decay values determined in the transduced interneuron were increased by several-fold over the uninfected control, resulting in an EPSC phenotype similar to that observed in mossy cells (Figures 2 and 6A). Analyses of the spontaneous EPSCs recordings from a total of 23 interneurons transduced with the +CNIH2 virus further extended on these effects on EPSC timing. Thus, the mean values determined for  $\tau$  EPSC decay ranged from 8.3 ms to 18.3 ms and yielded an overall mean ( $\pm$ SEM) for CNIH2-expressing interneurons of  $11.3 \pm 0.5$  ms

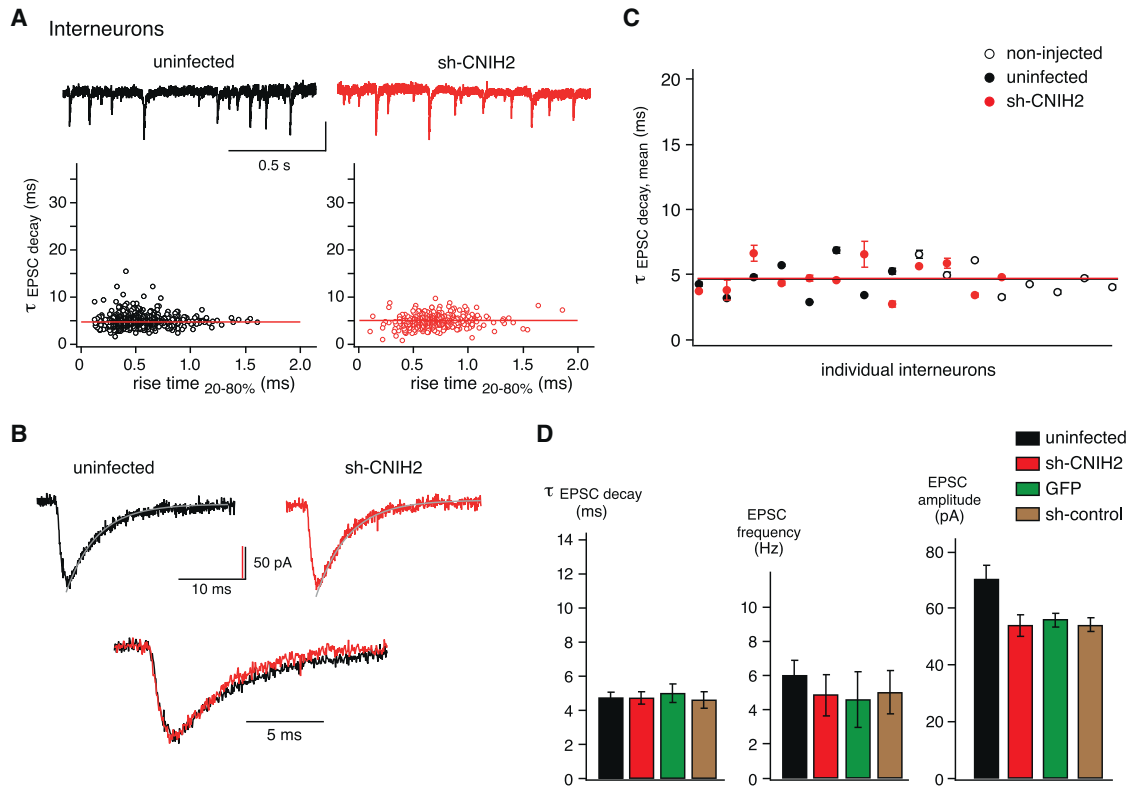


**Figure 5. CNIH2 Knockdown Did Not Affect EPSCs from Aspy Interneurons**

(A) Upper panel: spontaneous EPSCs recorded in an uninfected (left panel) and a sh-CNIH2-transduced interneuron (right panel). Time and current scaling as indicated. Lower panel: plot of  $\tau_{EPSC\ decay}$  versus rise time<sub>20%-80%</sub> determined from 596 (left) and 399 single EPSCs (right) from the cells above. Lines are linear fits to the data points with y values of 4.9 ms (left) and 5.2 ms (right).

(B) Single EPSCs recorded from the two cells above. Lines represent mono-exponential fits to the decay with values for  $\tau_{EPSC\ decay}$  of 4.6 ms (uninfected) and 4.8 ms (sh-CNIH2 transduced). Time and current scaling as indicated.

(C) Plot of the mean values ( $\pm$ SEM) of  $\tau_{EPSC\ decay}$  obtained in individual interneurons that were either transduced with sh-CNIH2 (red) or were uninfected controls. Lines are linear fits with y values of 4.6 ms (controls) and 4.7 ms (sh-CNIH2 transduced). All mean values were derived from 105 to 2,218 single EPSCs.

(D) Bar graph summarizing analyses of the indicated EPSC parameters. Bars represent mean  $\pm$ SEM of 20 (uninfected), 17 (sh-CNIH2-transduced), 5 (GFP-virus), and 5 (sh-control) interneurons.

(Figure 6B), a value very close to that obtained for mossy cells (Figure 3). Similar to the viral transductions above (Figure 5), the amplitudes of the EPSCs recorded from CNIH2-expressing interneurons were slightly smaller than those in uninfected control cells (Figure 6B).

These results identify CNIH2 as the determinant discriminating the EPSC phenotypes of hilar mossy cells and interneurons and show that CNIH2 expression slows EPSCs when integrated into postsynaptic AMPARs. Interestingly, transduction of mossy cells with the +CNIH2 virus did not result in appreciable changes of the EPSC parameters, suggesting that the CNIH2 protein is present at saturating levels in these neurons (Figure 6C).

### CNIH2 Knockdown in Individual MFB-Mossy Cell Synapses

Finally, we probed the relevance of CNIH2 for transmission at individual synapses by performing paired recordings between MFBs and either sh-CNIH2-transduced or control mossy cells. Figure 7A shows examples of EPSCs recorded in response to APs elicited in MFBs by a patch-pipette in whole-bouton config-

uration. Similar to spontaneous EPSCs, CNIH2 knockdown led to a marked acceleration of the EPSC decay (Figure 7A). The  $\tau_{EPSC\ decay}$  determined in individual synapses on uninfected mossy cells varied between 9.5 ms and 15.1 ms, yielding a mean value ( $\pm$ SD) of  $12.3 \pm 2.1$  ms ( $n = 16$  synapses), while in sh-CNIH2 transduced cells, the mean  $\tau_{EPSC\ decay}$  was  $5.4 \pm 1.1$  ms ( $n = 8$  synapses) with the decay in individual synapses scattering between 4.3 ms and 7.1 ms (Figure 7B). Thus, after knockdown of CNIH2 MFB-mossy cell synapses appeared very much like MFB-interneuron synapses, where synaptic AMPARs are devoid of CNIH2 (Figures 1C and 2).

In contrast to the changes in timing induced by sh-CNIH2, the EPSC amplitudes were similar between transduced and uninfected mossy cells, as were the paired pulse ratios, indicating that knockdown of CNIH2 selectively affected the gating of the postsynaptic AMPARs without altering the transmitter release probability (Figure 7B).

These results indicate that CNIH2 is responsible for the slow EPSC decay in MFB-mossy cell synapses and demonstrate the impact of this core subunit of postsynaptic AMPARs on the

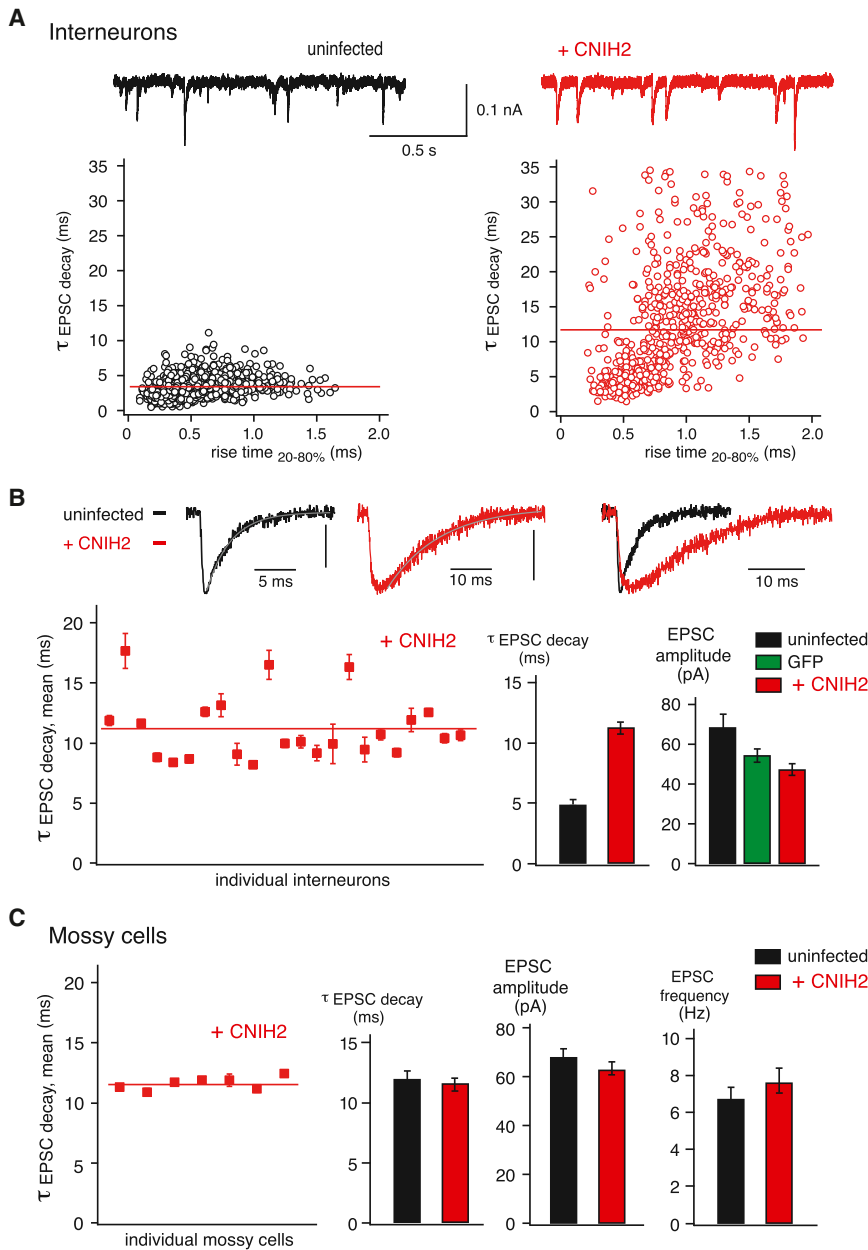


### Figure 6. Expression of CNIH2 in Aspiny Interneurons Converts Their EPSC Phenotype

(A) Upper panel: spontaneous EPSCs recorded from an uninfected aspiny interneuron (left panel) and one transduced with a virus driving expression of CNIH2 (+ CNIH2; right panel). Time and current scaling as indicated. Lower panel: plot of  $\tau$  EPSC decay versus rise time 20%–80% determined in 1,267 (open dots, left) and 670 single EPSCs (right) from the two interneurons above. Red lines are linear fits to the data points with y values of 3.7 ms (left) and 11.8 ms (right).

(B) Upper panel: single EPSCs recorded from the two cells above. Lines represent mono-exponential fits to the current decay with values for  $\tau$  EPSC decay of 3.1 ms (uninfected) and 12.6 ms (+ CNIH2). Time scaling as indicated; current scale is 50 pA. Lower left panel: plot of the mean values ( $\pm$ SEM) of  $\tau$  EPSC decay obtained from individual interneurons transduced with the CNIH2-expression virus. Line is a linear fit with a y value of 11.3 ms; mean values were derived from 12 to 828 single EPSCs. Lower right panels: bar graphs as in Figure 3C for the indicated parameters. Bars represent mean  $\pm$ SEM of 20 (uninfected), 5 (GFP-virus), and 23 (+CNIH2-transduced) interneurons.

(C) Left panel: plot of the mean values ( $\pm$ SEM) of  $\tau$  EPSC decay obtained from individual mossy cells transduced with the CNIH2-expression virus. Line is a linear fit with a y value of 11.4 ms; mean values were derived from 92 to 709 single EPSCs. Right panels: bar graphs as in (B) for the indicated parameters. Bars represent mean  $\pm$ SEM of 44 (uninfected) and 7 (+CNIH2-transduced) mossy cells.

time course of synaptic transmission. The extent of EPSC slowing accompanying CNIH2 parallels the effects found for the coassembly of CNIH2 with various GluA homo- and heterotetramers in heterologous expression experiments (Coombs et al., 2012; Kato et al., 2010; Schwenk et al., 2012; Schwenk et al., 2009; Shi et al., 2010).

## DISCUSSION

We demonstrated that CNIH2, an integral core subunit of native AMPARs (Schwenk et al., 2012), profoundly impacts the timing of synaptic transmission in hilar mossy cells of the hippocampus. In addition, CNIH2 is identified as the molecular distinction

between the slow EPSC phenotype observed in mossy cells and the fast EPSCs characteristic of interneurons.

### Relevance of CNIH2 for EPSC Timing

To dissect the role of CNIH2 for AMPAR-mediated excitatory synaptic transmission, we used paired recordings between presynaptic MFBs and two distinct postsynaptic target cells in combination with targeted protein knockdown via lenti-

virus-mediated shRNA expression. This combined approach permitted direct and precise investigation of EPSCs in individual synapses of manipulated and control neurons in the same slices.

Consistent with previous reports, the EPSCs recorded at MFB-mossy cell synapses displayed a prolonged decay time (Livsey and Vicini, 1992) (Figure 1). Interestingly, while the decay time was quite regular in any individual of the 50 synapses investigated, the absolute  $\tau$  EPSC decay values spanned a wide range among synapses differing by as much as 10 ms (Figure 1). Both the decay and the scattering range of the  $\tau$  EPSC decay were profoundly changed in mossy cells that experienced selective knockdown of CNIH2, a transmembrane protein that exclusively associates with the pore-forming GluA1-4 subunits of

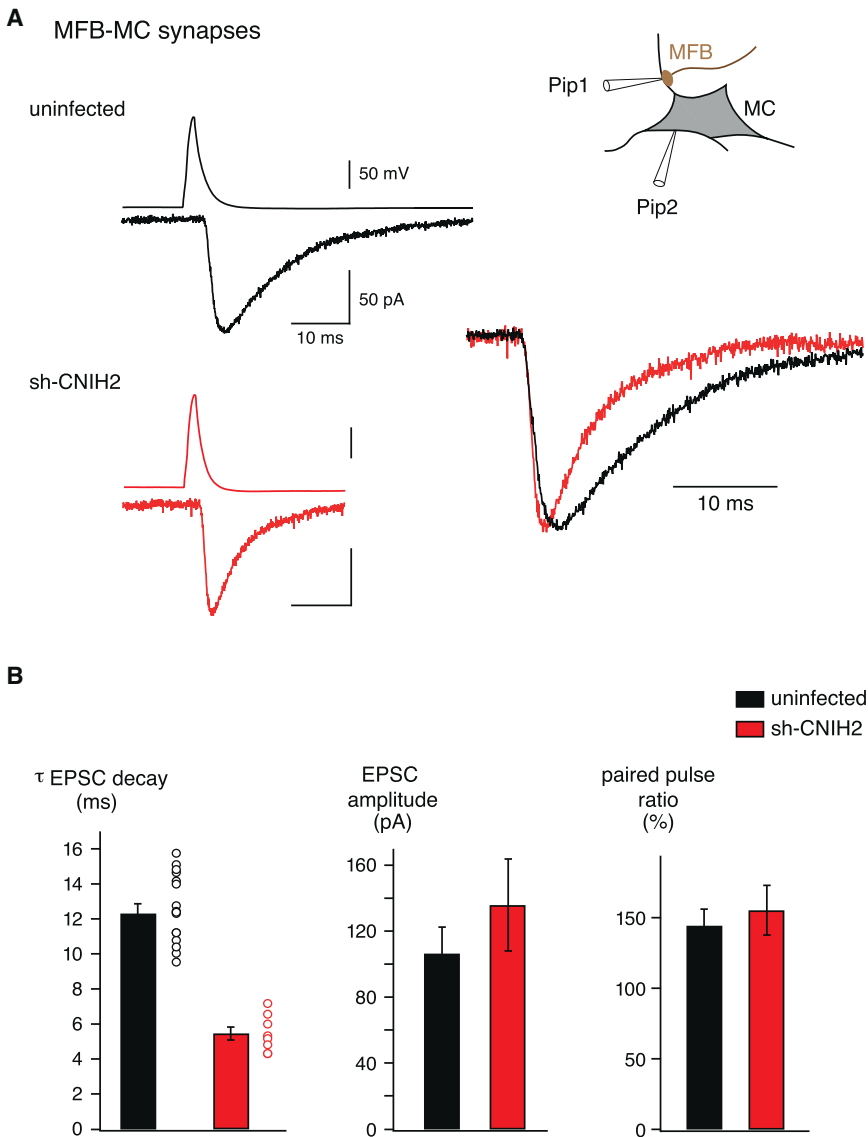


**Figure 7. CNIH2 Knockdown Speeds the Decay of EPSCs in Individual MFB-Mossy Cell Synapses**

(A) Left panel: representative paired recordings as in Figure 1 obtained in MFB-mossy cell synapses of uninfected and sh-CNIH2-transduced cells. Scaling for time, current, and voltage, as indicated. Right panel: overlay of the two evoked EPSCs on the left scaled to maximum. Values for  $\tau$  EPSC decay obtained by mono-exponential fits were 11.4 ms (uninfected) and 5.3 ms (sh-CNIH2).

(B) Bar graphs summarizing the EPSC analyses as in Figures 1 and 3. Data are mean  $\pm$  SEM of 17 (uninfected) and nine (sh-CNIH2) pairs. Open symbols in the left graph are values of  $\tau$  EPSC decay determined for the individual pairs. The paired pulse ratios were determined with 100 ms inter-pulse intervals.

AMPA receptors (over transmitter clearance or synapse morphology). Second, the variations in EPSC timing reflect the properties of synaptic AMPARs with distinct molecular composition. Third, postsynaptic CNIH2 expression profoundly impacts the gating of the AMPARs but does not affect their number in the postsynapse (Figures 3, 6, and 7). Fourth, the slowing of the AMPAR-mediated EPSCs provided by CNIH2 (Figures 2, 3, 6, and 7) is very close to the deceleration of AMPAR channel closing observed upon CNIH2 coexpression with various combinations of GluA pore-forming subunits (Coombs et al., 2012; Herring et al., 2013; Kato et al., 2010; Schwenk et al., 2009, 2012; Shi et al., 2010). Consequently, the prolonged time course of mossy cell EPSCs most likely results from CNIH2-containing AMPARs in the postsynaptic mem-

brane, while the faster EPSCs are mediated by AMPARs lacking CNIH2.

AMPARs (Schwenk et al., 2009, 2012). In fact, CNIH2 knockdown converted the characteristic mossy cell EPSC phenotype into a phenotype very similar to interneurons, with smaller values for  $\tau$  EPSC decay and markedly reduced variability, though clear synapse-to-synapse variation was still observed (Figures 1 and 7). Strikingly, the mossy cell phenotype of EPSCs was reconstituted with all characteristics in hilar interneurons upon expression of the CNIH2 protein (Figure 6). Noteworthy, all these changes in kinetics induced by the knockdown and (over) expression of CNIH2 occurred without any alterations in EPSC amplitude, and they were not accompanied by obvious changes in transmitter release probability or morphology of the presynapse (Figures 3, 6, and 7).

These findings provide important insights into the molecular mechanisms underlying the time course of synaptic transmission at hilar synapses. First, the EPSC time course is predominantly determined by the properties of the synaptic

brane, while the faster EPSCs are mediated by AMPARs lacking CNIH2.

The pronounced effects of CNIH2 knockdown or overexpression on the EPSC time course is not specific for mossy cells and interneurons in the hilus, as they were similarly observed in pyramidal cells of the CA3 and CA1 regions of the hippocampus (Figure S4). This is in line with a recent report by Herring et al. who also found an accelerated EPSC decay upon knockdown of CNIH2 in CA1 pyramidal cells (Herring et al., 2013). However, while we find no significant changes in the EPSC amplitude (Figures 1, 3, 7, and S4), they reported decreased amplitudes of synaptically evoked EPSCs, concomitant with an almost unchanged amplitude for miniature EPSCs. The authors suggested that these alterations result from the loss of surface GluA1-containing AMPARs due to an exclusive association of CNIH2 with GluA1, as they failed to detect CNIH2 in immunoprecipitations (IPs) of GluA2-containing AMPARs from *GluA1*<sup>-/-</sup> mice

(Herring et al., 2013). In contrast, our affinity purifications demonstrate robust assembly of CNIH2 into AMPARs in both *GluA1*<sup>-/-</sup> and *GluA2*<sup>-/-</sup> mice, albeit at lower amounts than in wild-type animals (Figure S1) (Schwenk et al., 2012). How can these differences be reconciled? The failure to detect CNIH2 in AMPAR IPs from *GluA1*-null mice is likely due to the use of the solvent Triton X-100 by Herring et al., as we previously showed that this detergent strongly interferes with the GluA-CNIH2 interactions (Figure 3 in Schwenk et al., 2012). The differences in EPSC amplitude may reflect the different experimental approaches: their use of mainly cultured slices and virally delivered, Cre-mediated gene disruption together with the extracellular stimulation technique, in contrast to our use of stereotactic injections in living rats to express shRNA and paired-bouton recordings in acute slice preparations.

### Implications for CNS Signaling

In the context of hilar circuits, the different EPSC kinetics are thought to contribute to the distinct specializations and the distinct input-output functions of these neurons (for review, Jinde et al., 2013; Scharfman and Myers, 2012). Thus, the CNIH2-mediated, longer-lasting EPSCs should promote more reliable propagation of the electrical signal and, together with the high-frequency input (about 800 granule cells synapse onto each mossy cell [Patton and McNaughton, 1995]), provide for robust output of the mossy cells onto granule cells (excitatory) and interneurons (inhibitory). Such reliable signaling by mossy cells has been implicated in pattern separation, storage and retrieval of information, and stability of microcircuits (Hyde and Strowbridge, 2012; Jinde et al., 2012; Leutgeb et al., 2007; Lisman, 1999). Conversely, the shorter lasting EPSCs resulting from CNIH2-free AMPARs specialize interneurons for precise coincidence detection and for precisely timed inhibitory input to granule cells (Freund and Buzsáki, 1996; Scharfman, 1992, 2007).

Beyond the significance for the two particular types of hilar neurons, the CNIH2-mediated distinction between slow and fast EPSC phenotypes is likely shared by other types of neurons in various brain regions where CNIH2 is expressed and relatively slow EPSCs have been described (Berretta and Jones, 1996; Geiger et al., 1995; Hestrin, 1993). In this respect, it will be interesting to probe the role of EPSC timing for information processing and output in neuronal circuits by manipulating expression of CNIH2. In conclusion, our results identify CNIH2 as a major determinant for the timing, and hence the efficacy, of synaptic transmission in the mammalian brain.

## EXPERIMENTAL PROCEDURES

### Molecular Biology

#### Generation of Lentiviruses for Expression of shRNAs

The oligonucleotide targeting rat CNIH2 (5'-AGCTGGTGGTCCCGGAATA; sh-CNIH2) and the control oligonucleotide (5'-TCGCTTGGGCGAGAGTAAG; sh-control) that does not target any gene transcript (Alberich-Jordà et al., 2012) were synthesized as sense-antisense hairpins and subcloned into pSuper (OligoEngine) downstream of the human H1 promoter. Using EcoRI/Clal, BstBI sites shRNA stretches were transferred to viral vectors (FUGW; Lois et al., 2002) equipped with EGFP under control of the human ubiquitin promoter. For coexpression of CNIH2 and GFP, a dual ubiquitin promoter system with

WPRES elements (Gascón et al., 2008) was integrated into the lentiviral FUGW vector. Lentiviruses were generated by transfecting tsa201 cells with transfer (pFUGW) and packaging (pVSV and pΔ8.9) vectors using the PEI transfection reagent. The medium was collected after 72 hr and filtered (0.45 μM) to remove cell debris. Virus particles were concentrated by centrifugation (24,500 rpm for 90 min; Beckman SW-32Ti) and suspended in artificial cerebrospinal fluid. Virus stock solutions had a titer of 10<sup>7</sup>–10<sup>8</sup>/ml.

Primary hippocampal neurons were prepared from rats at E18 and cultured as described (Goslin and Banker, 1989). Cells were transduced with lentivirus at DIV1 and cultivated for 3 weeks. The rate of infection was estimated based on the fluorescence of the EGFP marker included into the viral vectors (Figure S2).

### Electrophysiology

#### In Vivo Stereotactic Injection

The distinct lentiviruses were injected into Wistar rats 6–7 days after birth (P6–P7). Animals were anesthetized by injection of a ketamine/dorbene mixture and mounted in a Kopf stereotaxic frame (Tujunga). Virus-containing solution (0.5–2 μl) was injected at a single site targeting the hippocampus by means of a UMP3 controller (WPI, Sarasota) and a nanofil syringe/needle (WPI, Sarasota). Following surgery, pups recovered rapidly by antagonist injection and were returned to their home cage. Recordings were performed 10–18 days following virus injection. Animal procedures were in accordance with national and institutional guidelines and approved by the Animal Care Committee Freiburg according to the Tierschutzgesetz (AZ G-12/47).

#### Slice Preparation

Transverse 300-μm-thick hippocampal slices were cut from brains of 3- to 4-week-old Wistar rats, as described (Bischofberger et al., 2006). Hippocampal slices were cut in ice-cold, sucrose-containing physiological saline using a commercial vibratome (VT1200S, Leica Microsystems). Slices were incubated at 35°C, transferred into a recording chamber, and superfused with physiological saline at room temperature.

Cells and subcellular compartments (MFBs) were visualized by infrared differential interference contrast video microscopy using an Axio examiner microscope (Zeiss) equipped with a 63× water-immersion objective coupled to an epifluorescence system.

#### Cellular and Subcellular Patch-Clamp Recording

Patch pipettes were pulled from borosilicate glass (Hilgenberg; outer diameter, 2 mm; wall thickness, 0.7 mm for presynaptic recordings and 0.5 mm for somatic recordings). When filled with internal solution, they had resistances of ~15 MΩ (presynaptic pipettes) and 4–8 MΩ (postsynaptic pipettes). Patch pipettes were positioned using two Kleindiek micromanipulators (Kleindiek Nanotechnik, Reutlingen). A Multiclamp 700B amplifier (Molecular Devices, Sunnydale) was used for recordings. Pipette capacitance of both electrodes was compensated to 70%–90%. Voltage and current signals were filtered at 10 kHz with the built-in low-pass Bessel filter and digitized at 20 kHz using a Digidata 1440A (Molecular Devices, Sunnydale). pClamp10 software (Molecular Devices, Sunnydale) was used for stimulation and data acquisition.

#### Single and Paired Recordings

Simultaneous recordings were established between the soma of either a mossy cell or an aspiny interneuron and one MFB located in apposition to its dendrites (with a maximal distance of 60 μm from the soma). Both bouton-attached and whole-bouton configurations were used for eliciting APs that evoked synaptic transmission; APs were elicited by brief current pulses (2 ms, 200 pA). The postsynaptic neuron was held at –70 mV by injecting 0 to –200 pA holding current. EPSCs in individual MFB-mossy cell or MFB-interneuron synapses were determined as averages of 12–60 evoked EPSCs; thereby, latency of evoked EPSCs (delay between presynaptic AP and EPSC onset defined as 5% of peak amplitude) was between 0.2 and 2 ms. Spontaneous EPSCs were recorded from postsynaptic neurons that were held at –70 mV. Data for all conditions (uninjected, uninfected, and virally transduced) were recorded in brain slices obtained from at least three different animals from three different pups; recordings from virally transduced and noninfected control cells were performed in the same slices.

#### Solutions

For dissection and storage of slices, a sucrose-containing physiological saline containing 87 mM NaCl, 25 mM NaHCO<sub>3</sub>, 25 mM D-glucose, 75 mM sucrose,

2.5 mM KCl, 1.25 mM NaH<sub>2</sub>PO<sub>4</sub>, 0.5 mM CaCl<sub>2</sub>, and 7 mM MgCl<sub>2</sub> was used. Slices were superfused with physiological extracellular solution that contained 125 mM NaCl, 25 mM NaHCO<sub>3</sub>, 2.5 mM KCl, 1.25 mM NaH<sub>2</sub>PO<sub>4</sub>, 1 mM MgCl<sub>2</sub>, 2 mM CaCl<sub>2</sub>, and 25 mM glucose (equilibrated with a 95% O<sub>2</sub>/5% CO<sub>2</sub> gas mixture). Pipettes were filled with a K-methylsulfonate intracellular solution containing 120 mM KMeHSO<sub>3</sub>, 20 mM KCl, 2 mM MgCl<sub>2</sub>, 2 mM Na<sub>2</sub>ATP, 10 mM HEPES, and 0.1 mM EGTA.

Membrane potentials are given without correction for liquid junction potentials. Values given throughout the manuscript indicate mean  $\pm$  SEM or SD. Significance of differences was assessed by a nonparametric Mann-Whitney test.

#### Data Analysis

Stimfit 0.9 software and Igor Pro (WaveMetrics, Lake Oswego) were used to analyze data from spontaneous and evoked EPSCs. The rise time<sub>20%–80%</sub> was determined as the time interval between the points corresponding to 20% and 80% of the peak amplitude. The peak current was determined as the maximum within a 2 ms window following the presynaptic AP. For both single and paired recordings, the EPSC decay time constant ( $\tau_{EPSC\ decay}$ ) was obtained from a mono-exponential function fitted to the decay phase of the current (Livsey and Vicini, 1992). The analysis was restricted to spontaneous and evoked EPSCs fulfilling the following criteria: (1) the amplitude was larger than 30 pA (more than 2-fold larger than the noise recording), (2) the decay was complete (i.e., traces declined to baseline and were not interfered by further synaptic events; periods  $\geq$  40 ms) (i.e.,  $\geq$  40 ms), and (3) rise time<sub>20%–80%</sub> was between 0.4 and 2.0 ms.

#### Immunohistochemistry and Confocal Microscopy

Hilar neurons were filled during whole-cell recordings with 0.1% biocytin (Molecular Probes) added to the intracellular solution, MFBs were filled under the same conditions with Alexa 488 (Molecular Probes). After recordings, slices were fixed overnight at 4°C in 0.1 M phosphate buffer (PB) containing 4% paraformaldehyde. For immunohistochemistry, slices were incubated with rabbit *anti-CNIH2* primary antibody (Synaptic Systems; 1/50) overnight at 4°C in 0.3% Triton X-100 and 6% normal goat serum containing 0.1 M PB. Immunoreactions were visualized by goat anti-rabbit secondary antibody conjugated with Alexa 633, while biocytin-staining was revealed using Alexa 546-conjugated streptavidin. Cells and MFBs were investigated with a confocal laser-scanning microscope (LSM 710 meta, Zeiss) where confocal stacks were acquired with a Fluor 10 $\times$  0.5 N.A. and a Plan-Apochromat 40 $\times$  1.3 N.A. oil immersion objective (Zeiss).

Quantification of the shRNA effect in transduced slices (Figure S3) was performed with ImageJ software (<http://rsb.info.nih.gov/ij/>). Regions of interest corresponding to soma and proximal dendrites were manually framed either on the green channel (for selection of the virus-transduced GFP+ cells) or on the Far Red channel (for selection of the CNIH2-expressing cells not transduced with the virus [GFP-]) in the z stack exhibiting the largest area for the region of interest. Intensity of *anti-CNIH2* staining was collected for each cell; all intensities were corrected for background labeling. For quantification, the staining intensity of each sh-CNIH2-transduced cell was normalized to the mean value obtained from untransfected control cells expressing CNIH2 in each slice preparation.

#### Biochemistry

##### Membrane Preparation and Solubilization

Neurons were harvested at DIV21, lysed, and homogenized in ice-cold homogenization buffer (320 mM sucrose, 10 mM Tris/HCl [pH 7.5], 1.5 mM MgCl<sub>2</sub>, 1 mM EGTA, and 1 mM iodoacetamide) supplemented with protease inhibitors. Crude cell membrane fractions were obtained by ultracentrifugation (125,000  $\times$  g, 20 min.). Plasma-membrane-enriched protein fractions from isolated brains of adult mice (wild-type and knockout animals) were generated as described (Schwenk et al., 2012). Membrane proteins were solubilized for 30 min at 4°C with CL-47 or CL-91 (Logopharm GmbH, Germany) and non-solubilized proteins removed by ultracentrifugation (125,000  $\times$  g).

##### Affinity Purifications

A mixture of the following AMPAR antibodies was immobilized and incubated for 2 hr with respective membrane solubilizers: *anti-GluA1* (Millipore, #AB1504), *anti-GluA2* (NeuroMab, #75-002), *anti-GluA3* (Synaptic System,

#182-203), and *anti-GluA4* (Millipore, #AB1508). The complete pool of AMPAR complexes were pulled down (verified by western blotting) and after brief washing, bound proteins eluted and further processed for western blot and MS analyses (Schwenk et al., 2012). IgGs (Millipore, #12-370) were used as control.

Immunoblots were developed with the aforementioned *anti-GluA* antibodies, rabbit *anti-CNIH2* (raised against: DELRTDFKNPIDQGNPARARERLKNIERIC), *anti-TARP $\gamma$ -2/4/8* (NeuroMab, #75-252), *anti-GluN1* (SynapticSystem, #114.011), and *anti-Calnexin* (Abcam, #ab75801). Antibody stained bands were visualized by anti-mouse or anti-rabbit IgG-HRP (all Santa Cruz) and ECL prime (GE Healthcare).

##### Liquid Chromatography-Tandem Mass Spectrometry Analysis

Extracted postdigest peptide mixtures dissolved in 0.5% (v/v) trifluoroacetic acid were analyzed by nano-liquid chromatography-tandem mass spectrometry (LC-MS/MS) using a HPLC with C18 PepMap100 precolumn (5  $\mu$ m; Dionex) and analytical 75  $\mu$ m  $\times$  10 cm C18 column (PicoTip Emitter, 75  $\mu$ m, tip: 8  $\pm$  1  $\mu$ m, New Objective; self-packed with ReproSil-Pur 120 ODS-3, 3  $\mu$ m, Dr. Maisch) columns and an Orbitrap Elite mass spectrometer. PV-based quantifications and QconCAT standard calibrations were done as described in detail in Schwenk et al. (2012).

#### SUPPLEMENTAL INFORMATION

Supplemental Information includes four figures and can be found with this article online at <http://dx.doi.org/10.1016/j.neuron.2014.03.031>.

#### ACKNOWLEDGMENTS

We thank P. Jonas for instructive advice with the paired-bouton recording technique, J. Roeper for help with stereotactic injections, L. Dumont and I. Schaber for assistance, W. Bildl and U. Schulte for excellent support and help with MS-analyses, R. Sprengel for the gift of GluA knockout mice, and J.P. Adelman and G. Zolles for intense discussions and critical reading of the manuscript. This work was supported by grants of the DFG to B.F. (SFB 746, TP 16 and Fa 332/9-1).

Accepted: March 21, 2014

Published: May 21, 2014

#### REFERENCES

- Acsády, L., Kamondi, A., Sik, A., Freund, T., and Buzsáki, G. (1998). GABAergic cells are the major postsynaptic targets of mossy fibers in the rat hippocampus. *J. Neurosci.* 18, 3386–3403.
- Alberich-Jordá, M., Wouters, B., Balastik, M., Shapiro-Koss, C., Zhang, H., Di Ruscio, A., Radomska, H.S., Ebralidze, A.K., Amabile, G., Ye, M., et al. (2012). C/EBP $\gamma$  deregulation results in differentiation arrest in acute myeloid leukemia. *J. Clin. Invest.* 122, 4490–4504.
- Amaral, D.G. (1978). A Golgi study of cell types in the hilar region of the hippocampus in the rat. *J. Comp. Neurol.* 182, 851–914.
- Berretta, N., and Jones, R.S. (1996). A comparison of spontaneous EPSCs in layer II and layer IV-V neurons of the rat entorhinal cortex in vitro. *J. Neurophysiol.* 76, 1089–1100.
- Bildl, W., Haupt, A., Muller, C.S., Biniossek, M.L., Thumfart, J.O., Huber, B., Fakler, B., and Schulte, U. (2012). Extending the dynamic range of label-free mass spectrometric quantification of affinity purifications. *Mol. Cell Proteomics* 11, <http://dx.doi.org/10.1074/mcp.M111.007955>.
- Bischofberger, J., Engel, D., Li, L., Geiger, J.R., and Jonas, P. (2006). Patch-clamp recording from mossy fiber terminals in hippocampal slices. *Nat. Protoc.* 1, 2075–2081.
- Buckmaster, P.S., Wenzel, H.J., Kunkel, D.D., and Schwartzkroin, P.A. (1996). Axon arbors and synaptic connections of hippocampal mossy cells in the rat in vivo. *J. Comp. Neurol.* 366, 271–292.
- Conti, F., and Weinberg, R.J. (1999). Shaping excitation at glutamatergic synapses. *Trends Neurosci.* 22, 451–458.

- Coombs, I.D., Soto, D., Zonouzi, M., Renzi, M., Shelley, C., Farrant, M., and Cull-Candy, S.G. (2012). Cornichons modify channel properties of recombinant and glial AMPA receptors. *J. Neurosci.* *32*, 9796–9804.
- Farrant, M., and Cull-Candy, S.G. (2010). Neuroscience. AMPA receptors—another twist? *Science* *327*, 1463–1465.
- Freund, T.F., and Buzsáki, G. (1996). Interneurons of the hippocampus. *Hippocampus* *6*, 347–470.
- Frotscher, M., Seress, L., Schwerdtfeger, W.K., and Buhl, E. (1991). The mossy cells of the fascia dentata: a comparative study of their fine structure and synaptic connections in rodents and primates. *J. Comp. Neurol.* *312*, 145–163.
- Gascón, S., Paez-Gomez, J.A., Díaz-Guerra, M., Scheiffele, P., and Scholl, F.G. (2008). Dual-promoter lentiviral vectors for constitutive and regulated gene expression in neurons. *J. Neurosci. Methods* *168*, 104–112.
- Geiger, J.R., and Jonas, P. (2000). Dynamic control of presynaptic Ca<sup>2+</sup> inflow by fast-inactivating K<sup>+</sup> channels in hippocampal mossy fiber boutons. *Neuron* *28*, 927–939.
- Geiger, J.R., Melcher, T., Koh, D.S., Sakmann, B., Seeburg, P.H., Jonas, P., and Monyer, H. (1995). Relative abundance of subunit mRNAs determines gating and Ca<sup>2+</sup> permeability of AMPA receptors in principal neurons and interneurons in rat CNS. *Neuron* *15*, 193–204.
- Goslin, K., and Banker, G. (1989). Experimental observations on the development of polarity by hippocampal neurons in culture. *J. Cell Biol.* *108*, 1507–1516.
- Herring, B.E., Shi, Y., Suh, Y.H., Zheng, C.Y., Blankenship, S.M., Roche, K.W., and Nicoll, R.A. (2013). Cornichon proteins determine the subunit composition of synaptic AMPA receptors. *Neuron* *77*, 1083–1096.
- Hestrin, S. (1993). Different glutamate receptor channels mediate fast excitatory synaptic currents in inhibitory and excitatory cortical neurons. *Neuron* *11*, 1083–1091.
- Hollmann, M., and Heinemann, S. (1994). Cloned glutamate receptors. *Annu. Rev. Neurosci.* *17*, 31–108.
- Hyde, R.A., and Strowbridge, B.W. (2012). Mnemonic representations of transient stimuli and temporal sequences in the rodent hippocampus in vitro. *Nat. Neurosci.* *15*, 1430–1438.
- Isaac, J.T., Ashby, M.C., and McBain, C.J. (2007). The role of the GluR2 subunit in AMPA receptor function and synaptic plasticity. *Neuron* *54*, 859–871.
- Jinde, S., Zsiros, V., Jiang, Z., Nakao, K., Pickel, J., Kohno, K., Belforte, J.E., and Nakazawa, K. (2012). Hilar mossy cell degeneration causes transient dentate granule cell hyperexcitability and impaired pattern separation. *Neuron* *76*, 1189–1200.
- Jinde, S., Zsiros, V., and Nakazawa, K. (2013). Hilar mossy cell circuitry controlling dentate granule cell excitability. *Front. Neural Circuits* *7*, 14.
- Jonas, P. (2000). The time course of signaling at central glutamatergic synapses. *News Physiol. Sci.* *15*, 83–89.
- Kato, A.S., Gill, M.B., Ho, M.T., Yu, H., Tu, Y., Siuda, E.R., Wang, H., Qian, Y.W., Nisenbaum, E.S., Tomita, S., and Brecht, D.S. (2010). Hippocampal AMPA receptor gating controlled by both TARP and cornichon proteins. *Neuron* *68*, 1082–1096.
- Leutgeb, J.K., Leutgeb, S., Moser, M.B., and Moser, E.I. (2007). Pattern separation in the dentate gyrus and CA3 of the hippocampus. *Science* *315*, 961–966.
- Lisman, J.E. (1999). Relating hippocampal circuitry to function: recall of memory sequences by reciprocal dentate-CA3 interactions. *Neuron* *22*, 233–242.
- Livsey, C.T., and Vicini, S. (1992). Slower spontaneous excitatory postsynaptic currents in spiny versus aspiny hilar neurons. *Neuron* *8*, 745–755.
- Lois, C., Hong, E.J., Pease, S., Brown, E.J., and Baltimore, D. (2002). Germline transmission and tissue-specific expression of transgenes delivered by lentiviral vectors. *Science* *295*, 868–872.
- Milstein, A.D., Zhou, W., Karimzadegan, S., Brecht, D.S., and Nicoll, R.A. (2007). TARP subtypes differentially and dose-dependently control synaptic AMPA receptor gating. *Neuron* *55*, 905–918.
- Mosbacher, J., Schoepfer, R., Monyer, H., Burnashev, N., Seeburg, P.H., and Ruppersberg, J.P. (1994). A molecular determinant for submillisecond desensitization in glutamate receptors. *Science* *266*, 1059–1062.
- Patton, P.E., and McNaughton, B. (1995). Connection matrix of the hippocampal formation: I. The dentate gyrus. *Hippocampus* *5*, 245–286.
- Raman, I.M., and Trussell, L.O. (1992). The kinetics of the response to glutamate and kainate in neurons of the avian cochlear nucleus. *Neuron* *9*, 173–186.
- Sah, P., Hestrin, S., and Nicoll, R.A. (1990). Properties of excitatory postsynaptic currents recorded in vitro from rat hippocampal interneurons. *J. Physiol.* *430*, 605–616.
- Scharfman, H.E. (1992). Differentiation of rat dentate neurons by morphology and electrophysiology in hippocampal slices: granule cells, spiny hilar cells and aspiny ‘fast-spiking’ cells. *Epilepsy Res. Suppl.* *7*, 93–109.
- Scharfman, H.E. (2007). The CA3 “backprojection” to the dentate gyrus. *Prog. Brain Res.* *163*, 627–637.
- Scharfman, H.E., and Myers, C.E. (2012). Hilar mossy cells of the dentate gyrus: a historical perspective. *Front. Neural Circuits* *6*, 106.
- Schwenk, J., Harmel, N., Zolles, G., Bildl, W., Kulik, A., Heimrich, B., Chisaka, O., Jonas, P., Schulte, U., Fakler, B., and Klöcker, N. (2009). Functional proteomics identify cornichon proteins as auxiliary subunits of AMPA receptors. *Science* *323*, 1313–1319.
- Schwenk, J., Harmel, N., Brechet, A., Zolles, G., Berkefeld, H., Müller, C.S., Bildl, W., Baehrens, D., Hüber, B., Kulik, A., et al. (2012). High-resolution proteomics unravel architecture and molecular diversity of native AMPA receptor complexes. *Neuron* *74*, 621–633.
- Seeburg, P.H. (1993). The TINS/TiPS Lecture. The molecular biology of mammalian glutamate receptor channels. *Trends Neurosci.* *16*, 359–365.
- Shi, Y., Suh, Y.H., Milstein, A.D., Isozaki, K., Schmid, S.M., Roche, K.W., and Nicoll, R.A. (2010). Functional comparison of the effects of TARPs and cornichons on AMPA receptor trafficking and gating. *Proc. Natl. Acad. Sci. USA* *107*, 16315–16319.
- Silver, R.A., Traynelis, S.F., and Cull-Candy, S.G. (1992). Rapid-time-course miniature and evoked excitatory currents at cerebellar synapses in situ. *Nature* *355*, 163–166.
- Sobolevsky, A.I., Rosconi, M.P., and Gouaux, E. (2009). X-ray structure, symmetry and mechanism of an AMPA-subtype glutamate receptor. *Nature* *462*, 745–756.
- Szabadics, J., and Soltesz, I. (2009). Functional specificity of mossy fiber innervation of GABAergic cells in the hippocampus. *J. Neurosci.* *29*, 4239–4251.
- Tomita, S., Chen, L., Kawasaki, Y., Petralia, R.S., Wenthold, R.J., Nicoll, R.A., and Brecht, D.S. (2003). Functional studies and distribution define a family of transmembrane AMPA receptor regulatory proteins. *J. Cell Biol.* *161*, 805–816.
- Trussell, L.O. (1999). Synaptic mechanisms for coding timing in auditory neurons. *Annu. Rev. Physiol.* *61*, 477–496.